

**Short-pulse photoassociation in rubidium below the  $D_1$  line**

Christiane P. Koch\* and Ronnie Kosloff

*Department of Physical Chemistry and The Fritz Haber Research Center, The Hebrew University, Jerusalem 91904, Israel*

Françoise Masnou-Seeuws

*Laboratoire Aimé Cotton, CNRS, Bât. 505, Campus d'Orsay, 91405 Orsay Cedex, France*

(Received 28 November 2005; published 13 April 2006)

Photoassociation of two ultracold rubidium atoms and the subsequent formation of stable molecules in the singlet ground and lowest triplet states is investigated theoretically. The method employs laser pulses inducing transitions via excited states correlated to the  $5S+5P_{1/2}$  asymptote. Weakly bound molecules in the singlet ground or lowest triplet state can be created by a single pulse while the formation of more deeply bound molecules requires a two-color pump-dump scenario. More deeply bound molecules in the singlet ground or lowest triplet state can be produced only if efficient mechanisms for both pump and dump steps exist. While long-range  $1/R^3$  potentials allow for efficient photoassociation, stabilization is facilitated by the resonant spin-orbit coupling of the  $0_u^+$  states. Molecules in the singlet ground state bound by a few wave numbers can thus be formed. This provides a promising first step toward ground-state molecules which are ultracold in both translational and vibrational degrees of freedom.

DOI: [10.1103/PhysRevA.73.043409](https://doi.org/10.1103/PhysRevA.73.043409)

PACS number(s): 33.80.Ps, 32.80.Qk, 34.50.Rk

**I. INTRODUCTION**

The formation of ultracold molecules along with the creation of molecular Bose-Einstein condensates (BEC's) [1–3] opens the way to a new field of research [4]. Methods to directly cool the translational degrees of freedom of molecules have advanced significantly over the last few years. However, the lowest temperatures to date have been achieved by cooling atoms and then assembling the atoms into molecules by applying an external field. To this end, magnetic as well as optical fields have been employed. The formation of weakly bound alkali-metal dimer molecules with magnetic fields using so-called Feshbach resonances has been particularly successful; see, e.g., [5–7]. Optical techniques, however, present a very general technique due to the abundance and diversity of optical transitions. Furthermore, laser fields can be manipulated, offering various possibilities for control. In particular, molecules in their vibronic ground state can be created by employing a combination of light fields of different colors [8]. The major drawback of optical techniques is the fairly short lifetime of the electronic states involved, on the order of a few tens of nanoseconds for the alkali-metal dimer systems. The coherence of the control process may then be lost because of spontaneous emission [9,10]. This flaw, which is particularly severe in view of creating a stable molecular BEC, can be overcome by employing laser pulses with a duration shorter than the excited state lifetimes.

The use of short laser pulses offers several advantages in the manipulation of ultracold systems. Obviously the shorter time scale can overcome the losses induced by spontaneous emission. In addition, a sequence of shaped pulses can control the photoassociation mechanism. Two time-delayed

pulses can be employed to realize pump-probe experiments: The first or pump pulse creates a wave packet whose dynamics is monitored by a second probe pulse, varying the time delay [11,12]. The shape of the pulse can be manipulated, for example, by introducing a controlled frequency chirp which enforces adiabatic following conditions [13–16]. More elaborate coherent control which shapes the amplitude and phase can also be employed. These pulses can be found using feedback learning loops [17]. The underlying idea is to employ information on quantum interferences to construct a pulse which is able to steer the process into the desired direction [18]. However, the know-how of closed-loop, coherent-control experiments [17] cannot be transferred to experiments on ultracold systems in a one-to-one fashion. This is because the dynamical time scales of cold systems are simply much larger than the femtosecond time scale of lasers suitable for coherent control. The adaptation of pulse shaping techniques known from coherent control to ultracold systems is a subject of current investigation [19,20]. In addition to controlling nuclear dynamics, a femtosecond laser can be employed for high-resolution spectroscopy in ultracold systems by utilizing it as a frequency comb [21]. These two limits have recently been combined in a spectroscopic study with coherent-pulse accumulation [22]. The appeal of such an approach lies in the fact that with a femtosecond-frequency comb it is possible to continuously switch between the two limits, selecting the desired time and frequency resolution.

Photoassociation (PA) was originally developed with continuous-wave (cw) lasers, allowing for high-precision spectroscopy [23,24]. PA with short laser pulses does not yield spectroscopic information and requires theoretical modeling. In general, PA is defined as the formation of electronically excited molecules from two colliding atoms by interaction with laser light. In a subsequent stabilization step, molecules in the singlet ground state or in the lowest triplet state are created by spontaneous or stimulated emission. Pho-

\*Electronic address: ckoch@fh.huji.ac.il

toassociation with short laser pulses on cold systems has sparked interest from both experiment [8,16,19,20] and theory [13–15,25–27]. Specifically, a pump-dump scheme has been suggested with the idea to create a wave packet on the excited state and make use of its time dependence for efficient stabilization [14,15,27]. In order to obtain an overall high efficiency, both excitation (photoassociation) and deexcitation (stabilization) steps must be efficient. PA can be understood as a vertical transition at the Franck-Condon distance  $R_C$  depending on the frequency  $\omega_p$  or detuning  $\Delta_p$ . It works best at long range [23,24]. Since excitation of the atomic resonance needs to be avoided, this requires a rather narrow bandwidth—i.e., pulses in the picosecond to nanosecond regime. The efficiency of the stabilization step depends on the topology of the potentials and the time delay between pump and dump pulses [27]. In PA experiments with cw lasers, the stabilization step is determined only by the potentials and the transition dipole moment—i.e., by the Franck-Condon factors of single excited-state vibrational levels. In a time-dependent process the excited-state wave packet is made up of a superposition of several vibrational levels and moves under the influence of the excited-state potential. This movement can also be viewed as interferences in time of the superposition coefficients. Stabilization is most effective if the dump pulse interacts with the molecular wave packet when it is located at short internuclear distances. For cesium it was found that up to 20% of the excited-state wave packet can be transferred to molecules in the lowest triplet state [27].

The present study employs the concepts developed in Refs. [13–16] for PA with chirped pulses and of Ref. [27] for the pump-dump scheme. In previous work on cesium, only excitation of the  $0_g^-(P_{3/2})$  excited state and molecule formation in the lowest triplet state  $a^3\Sigma_u^+$  were considered [27]. In order to analyze short pulse PA from the point of view of a prospective experiment, the present study goes beyond the two-state description [13–16,27]. Formation of molecules in both the singlet ground state  $X^1\Sigma_g^+$  and the lowest triplet state  $a^3\Sigma_u^+$  can then be tested. Rubidium has been chosen since experimental effort is under way for this species [19,20]. A comprehensive model of the interaction of two atoms with a laser field is developed, and the role of all laser parameters is analyzed. In particular, due to the bandwidth of the pulse, a number of vibrational levels of the electronically excited state are excited. These levels may belong to different electronic states. For this reason all potentials which allow for transitions within the bandwidth of the pulse are included in the model. For the sake of brevity, the focus is on the potentials correlated to the  $5S+5P_{1/2}$  atomic asymptote—i.e., to the  $D_1$  line. The corresponding model will be introduced in Sec. II. Considering transitions into  $5S+5P_{1/2}$  potentials implies that the central frequency of the laser is red detuned from the  $D_1$  line. The control knobs which can be varied in the experiment are the parameters of the laser pulse—i.e., its central frequency, spectral bandwidth, intensity, and possibly frequency chirp. The variation of these parameters will guide the discussion of the mechanisms of excitation and deexcitation in Secs. III and IV, respectively. The separation of pump and dump mechanisms is not only a convenience of the theoretical discussion. It is

motivated by the fact that the two steps correspond to two different detection schemes in an experiment: The excitation of two colliding atoms into long-range, electronically excited molecules would be measured as trap loss of the atomic cloud while the formation of molecules in the singlet ground and lowest triplet states would be monitored by resonantly enhanced multiphoton ionization (REMPI) spectroscopy. Accurate information from *ab initio* calculations and spectroscopy for the molecular potentials and transition dipole moments is employed in the current study. Unfortunately, no such data are available as yet for the description of the spin-orbit coupling. Therefore three different model curves are employed, and the sensitivity of the proposed scheme with respect to the spin-orbit coupling is discussed in Sec. V. Finally, conclusions are drawn in Sec. VI. In particular, the experimental feasibility of creating ultracold stable molecules with short-pulse PA is discussed.

## II. MODEL

Two colliding rubidium-87 atoms in their ground state ( $5S+5S$ ) interacting with a laser field are considered. The laser excites the two atoms into an electronically excited state ( $5S+5P$ ) which may support long-range molecular bound levels. Four  $\Sigma^+$  and four  $\Pi$  [Hund's case (a)] states (singlet-triplet and gerade-ungerade states) are correlated to the  $5S+5P$  asymptote, with two of them repulsive and two attractive. When including the spin-orbit interaction (see, e.g., [28]), the respective 0, 1, and 2 [Hund's case (c)] potentials are obtained. Five of these are correlated to the  $5S+5P_{1/2}$  asymptote—i.e., the  $D_1$  line. Out of these five, only the attractive potentials  $0_u^+(P_{1/2})$ ,  $1_g(P_{1/2})$ , and  $0_g^-(P_{1/2})$  which support bound molecular levels are considered. For the  $0_u^+$  states, the spin-orbit coupling has resonant character [29–31] and leads to an avoided crossing between  $0_u^+(P_{1/2})$  and  $0_u^+(P_{3/2})$  at short internuclear distance. The spin-orbit coupling therefore needs to be included explicitly: The Hund's-case (c) potentials are obtained by diagonalizing the Hamiltonian containing the Hund's-case (a) potentials on the diagonal and the spin-orbit coupling on the off diagonal [28]. The corresponding unitary transformation leads to off-diagonal elements of the kinetic energy which usually are neglected. For resonant coupling, however, these “nonadiabatic couplings” have to be taken into account: In the case of the two  $0_u^+(P_{3/2})$  and  $0_u^+(P_{1/2})$  curves, it couples the two vibrational series and leads to well-known perturbations in the spectra [29].

Due to conservation of the gerade-ungerade symmetry in homonuclear dimer molecules, optical transitions are allowed to  $0_u^+$  from the singlet  $X^1\Sigma_g^+$  ground state and to  $1_g$  and  $0_g^-$  from the  $a^3\Sigma_u^+$  lowest triplet state. For the interaction with the field, the dipole and rotating-wave approximations are assumed. The  $0_u^+(P_{1/2})$ ,  $1_g(P_{1/2})$ , and  $0_g^-(P_{1/2})$  states on the one hand and the  $X^1\Sigma_g^+$  and  $a^3\Sigma_u^+$  states on the other hand are coupled by a hyperfine interaction. However, since the time scale associated with the hyperfine interaction is much larger than the time scales of femtosecond and picosecond pulses, the coupling between the states can be neglected, and three separate Hamiltonians  $\hat{H}_1$ ,  $\hat{H}_2$ , and  $\hat{H}_3$  will be considered.

The Hamiltonian  $\hat{H}_1$  which describes transitions from the singlet ground state into the  $0_u^+$  excited states is given by

$$\hat{H}_1 = \begin{pmatrix} \hat{T} + V_{X^1\Sigma_g^+}(\hat{\mathbf{R}}) & \mu_\pi(\hat{\mathbf{R}})E(t) & 0 \\ \mu_\pi(\hat{\mathbf{R}})E(t) & \hat{T} + V_{A^1\Sigma_u^+}(\hat{\mathbf{R}}) - \hbar\omega_L & \sqrt{2}W_{SO}(\hat{\mathbf{R}}) \\ 0 & \sqrt{2}W_{SO}(\hat{\mathbf{R}}) & \hat{T} + V_{b^3\Pi_u}(\hat{\mathbf{R}}) - W_{SO} - \hbar\omega_L \end{pmatrix}, \quad (1)$$

where  $\hat{T}$  denotes the kinetic energy operator and  $V_i(\hat{\mathbf{R}})$  the respective potential energy curves. The scalar product between the transition dipole moment and the polarization vector of the field is denoted as  $\mu_{\sigma(\pi)}(\hat{\mathbf{R}})$  for  $\sigma$  ( $\pi$ ) polarization. The laser field is characterized by its temporal shape and central frequency,  $E(t)\exp(i\omega_L t)$ . The  $\hat{\mathbf{R}}$  dependence of the spin-orbit coupling  $W_{SO}$  is not known. It is therefore approximated by its asymptotic value,  $W_{SO} = \text{const} = 1/3\Delta E_{FS}$ , which is given in terms of the fine structure splitting,  $\Delta E_{FS}$

$= 237.5984 \text{ cm}^{-1}$  for rubidium. In Sec. V, two different model curves for  $W_{SO}(\hat{\mathbf{R}})$  will be introduced and the dependence of the results on the specific description of the spin-orbit coupling will be discussed.

For the  $1_g$  and  $0_g^-$  states, the spin-orbit coupling has not got resonant character. In order to treat them on the same level of rigor as  $0_u^+$ , the spin-orbit interaction is nonetheless included explicitly as in Eq. (1). The Hamiltonians  $\hat{H}_2$  and  $\hat{H}_3$  then read

$$\hat{H}_2 = \begin{pmatrix} \hat{T} + V_{a^3\Sigma_u^+}(\hat{\mathbf{R}}) & \mu_\sigma(\hat{\mathbf{R}})E(t) & 0 & \mu_\pi(\hat{\mathbf{R}})E(t) \\ \mu_\sigma(\hat{\mathbf{R}})E(t) & \hat{T} + V_{3\Pi_g}(\hat{\mathbf{R}}) - \hbar\omega_L & W_{SO}(\hat{\mathbf{R}}) & W_{SO}(\hat{\mathbf{R}}) \\ 0 & W_{SO}(\hat{\mathbf{R}}) & \hat{T} + V_{1\Pi_g}(\hat{\mathbf{R}}) - \hbar\omega_L & -W_{SO}(\hat{\mathbf{R}}) \\ \mu_\pi(\hat{\mathbf{R}})E(t) & W_{SO}(\hat{\mathbf{R}}) & -W_{SO}(\hat{\mathbf{R}}) & \hat{T} + V_{3\Sigma_g^+}(\hat{\mathbf{R}}) - \hbar\omega_L \end{pmatrix} \quad (2)$$

and

$$\hat{H}_3 = \begin{pmatrix} \hat{T} + V_{a^3\Sigma_u^+}(\hat{\mathbf{R}}) & \mu_\pi(\hat{\mathbf{R}})E(t) & \mu_\sigma(\hat{\mathbf{R}})E(t) \\ \mu_\pi(\hat{\mathbf{R}})E(t) & \hat{T} + V_{3\Sigma_g^+}(\hat{\mathbf{R}}) - \hbar\omega_L & \sqrt{2}W_{SO}(\hat{\mathbf{R}}) \\ \mu_\sigma(\hat{\mathbf{R}})E(t) & \sqrt{2}W_{SO}(\hat{\mathbf{R}}) & \hat{T} + V_{3\Pi_g}(\hat{\mathbf{R}}) - W_{SO} - \hbar\omega_L \end{pmatrix}. \quad (3)$$

Both  $1_g$  and  $0_g^-$  states are coupled to the lowest triplet state by  $\sigma$  as well as  $\pi$  polarization. For simplicity the nuclear axis is chosen to be *either* parallel or perpendicular to the polarization axis of the laser field. For an ensemble of atoms in a magneto-optical trap (MOT) with no preferred axis, an average over all angles between the nuclear and polarization axes needs to be performed. This is beyond the scope of the current study. Furthermore, rotational excitation is presently neglected and will be addressed in future work.

The potentials  $V_i(\hat{\mathbf{R}})$  have been obtained by matching the results of *ab initio* calculations [32] to the long-range dispersion potentials ( $C_3/\hat{\mathbf{R}}^3 + C_6/\hat{\mathbf{R}}^6 + C_8/\hat{\mathbf{R}}^8$  (see Ref. [33] for details of the *ab initio* calculations). The coefficients for the  $5S+5S$  asymptote are found in Ref. [34], while the coefficients for the  $5S+5P$  asymptote are taken from Ref. [35]. The repulsive barrier of the ( $5S+5S$ ) potentials has been ad-

justed to give a triplet (singlet) scattering length of  $99a_0$  ( $90a_0$ ). The excited-state potentials in both Hund's-case (a) and (c) representations are shown in Fig. 1. Note that at long range the  $0_g^-(P_{1/2})$  potential goes as  $1/R^6$  since the  $1/R^3$  terms cancel each other. For the  $1_g$  and  $0_g^-$  states, the spin-orbit coupling influences mostly the long-range part of the potentials while at short range the singlet (triplet) character is retained. For the  $0_u^+$  potentials, however, resonant coupling between the  $A^1\Sigma_u^+$  and  $b^3\Pi_u^+$  states is observed which is due to the (avoided) crossing at  $R \approx 9.5a_0$  (see inset in Fig. 1). The  $0_u^+$  vibrational eigenfunctions therefore have mixed singlet-triplet character over a large range of binding energies. The  $\hat{\mathbf{R}}$ -dependent transition dipole moments are also taken from the *ab initio* calculations [32].

The Hamiltonians, Eqs. (1)–(3), are represented on a grid employing a mapped-grid method [30,36]. This allows one to

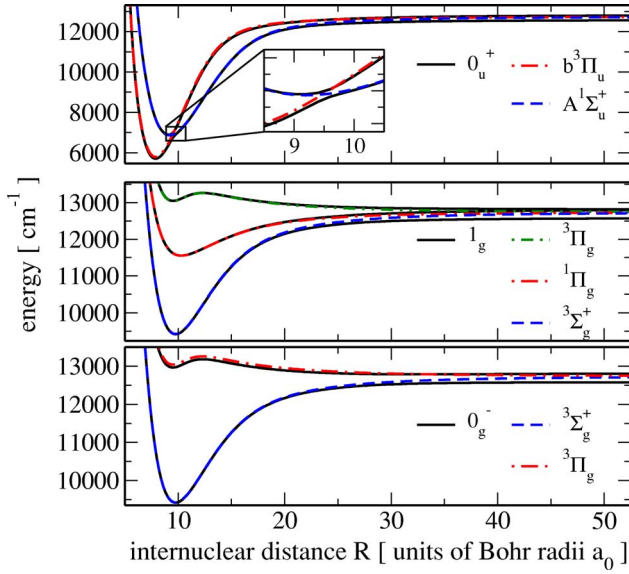


FIG. 1. (Color online) The three potentials correlated to the  $D_1$  line into which dipole-allowed transitions may occur:  $0_u^+$ ,  $1_g$ , and  $0_g^-$  (black solid lines). Also shown are their counterparts which are correlated to the  $D_2$  line and the corresponding Hund's-case (a) potentials (red, blue, and green dashed and dash-dotted lines).

employ a fairly extended grid ( $R_{\max} \approx 18\,500a_0$ ) with a comparatively small number of grid points ( $N_{\text{grid}}=1024$ ). Such a large grid is needed to faithfully represent the scattering continuum above the singlet-ground- and lowest triplet-state potentials by box states [14,15,27]. Diagonalization of the Hamiltonians, Eqs. (1)–(3), with  $E(t)$  set to zero gives the vibrational energy levels and wave functions. Figure 2 shows an example of these eigenfunctions of the  $0_u^+$  and  $1_g$  states. Some of the  $0_u^+$  eigenfunctions are strongly perturbed by the resonant coupling (shown on the left-hand side of Fig. 2; see also Ref. [30]) as compared to the regular vibrational wave functions shown for the  $1_g$  state. Note that the peak at  $R=25$  a.u. in the wave functions on the left-hand side of Fig. 2 corresponds to the outer turning point of the  $0_u^+(P_{3/2})$  potential.

The time-dependent Schrödinger equation

$$i\hbar \frac{\partial}{\partial t} |\Psi(t)\rangle = \hat{H}(t) |\Psi(t)\rangle \quad (4)$$

is solved with a Chebychev propagator. Coherent effects resulting from laser pulses which overlap in time are not of interest in the current context. Therefore the excitation and deexcitation steps are treated separately. In the first step, an initial scattering state is excited by a PA (pump) pulse. After a certain time delay a second (dump) pulse, suitably frequency shifted with respect to the first one, transfers the excited-state population back to the electronic ground state. Both laser pulses are assumed to have a Gaussian envelope and possibly a frequency chirp,

$$E_j(t) = \frac{E_{0,j}}{\sqrt{f_j}} e^{-(t-t_j)^2/2\sigma_j^2} e^{i(\chi_j/2)(t-t_j)^2} \quad (j=P,D). \quad (5)$$

The Gaussian standard deviation  $\sigma_{P(D)}$  is related to the full width at half maximum (FWHM) of the intensity profile

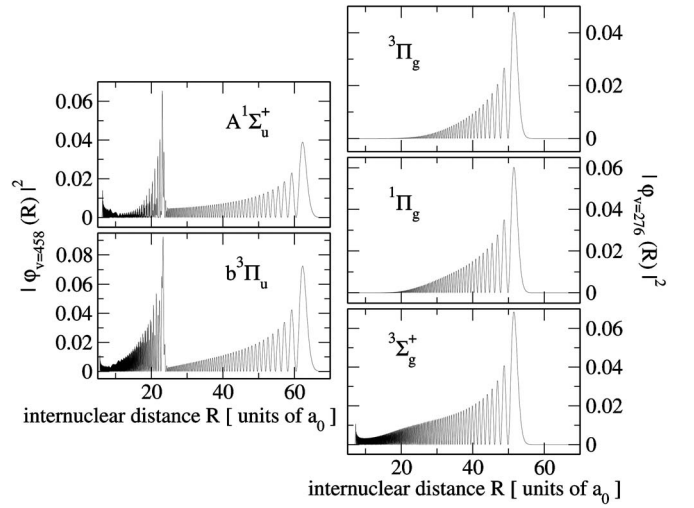


FIG. 2. Vibrational wave functions of the  $0_u^+$  (left) and  $1_g$  (right) potentials with binding energies of  $10.3\text{ cm}^{-1}$  and  $10.2\text{ cm}^{-1}$  with respect to the  $D_1$  line.

$\tau_{P(D)}$  of the pump (dump) pulse by  $\tau_{P(D)} = 2\sqrt{\ln 2} \sigma_{P(D)}$ .  $t_{P(D)}$  denotes the time at which the field amplitude is maximum, and  $\chi_{P(D)}$  is the time chirp of the pump (dump) pulse. The stretch factor  $f_{P(D)}$  gives the ratio between the pulse duration of the chirp to that of the corresponding transform-limited pulse,  $f = \tau^{\text{chirp}} / \tau^{\text{tl}}$  ( $f_j=1$  for transform-limited pulses). Some of the parameters characterizing a chirped pulse are related. While chirping stretches the pulse in time, it leaves its spectral bandwidth (FWHM)  $\Delta\omega$  invariant,  $\Delta\omega = 2\sqrt{\ln 2} \Gamma$ , with  $\Gamma$  the Gaussian standard deviation of the Fourier transform of  $E_j(t)e^{-i\omega_j t}$ ,

$$\tilde{E}_j(\omega) = E(\omega_j) e^{(\omega - \omega_j)^2/2\Gamma^2} e^{i\Phi_j(\omega - \omega_j)^2/2} \quad (6)$$

( $j=P,D$ ), and  $\Gamma = 2/\sigma^{\text{tl}}$ . Time and frequency domain chirps are related to the spectral bandwidth via

$$\chi = \frac{\sqrt{f^2 - 1} \Gamma^2}{f^2} \frac{4}{4}, \quad \Phi = \sqrt{f^2 - 1} \frac{4}{\Gamma^2}.$$

In the following, a pulse will be characterized by its central frequency  $\omega_j$  (or, respectively, detuning from the  $D_1$  line,  $\Delta_j$ ), FWHM  $\tau_j$  of the transform-limited pulse (implying its spectral bandwidth  $\Delta\omega_j$ ), stretch factor  $f_j$  which gives the strength of the chirp, the sign of the chirp, and the pulse energy. The latter is related to the maximum pulse amplitude  $E_j$  and to the duration  $\sigma_j$  by

$$\mathcal{E}_j = \varepsilon_0 c \sqrt{\pi} \pi r^2 E_j^2 \sigma_j,$$

with  $\varepsilon_0$  the electric constant,  $c$  the speed of light, and  $r$  the radius of the laser beam ( $r=300\ \mu\text{m}$  is assumed throughout this work). These parameters are chosen to correspond to pulses which can be generated from a femtosecond oscillator without amplification. This implies in particular pulses with FWHM of up to 10 ps and pulse energies of a few nanojoule corresponding to peak intensities on the order of  $100\text{ kW/cm}^2$ .

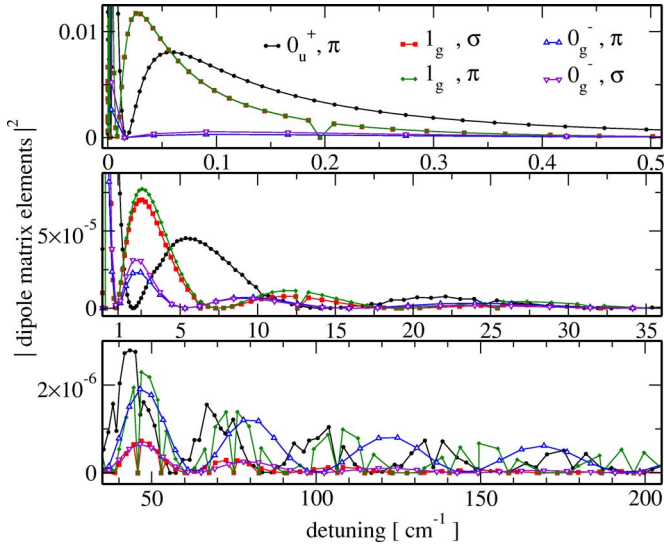


FIG. 3. (Color online) Dipole matrix elements (absolute values squared) between an initial scattering state of two atoms with collision energy corresponding to  $T=105 \mu\text{K}$  and excited-state vibrational levels vs binding energy equal to the photoassociation laser detuning. The scattering state is normalized to 1 (see text for further explanations). Different electronic states are compared (the required polarization is denoted in the legend). *The DPM elements are similar for transitions to  $0_u^+$  and  $1_g$  for all detunings. For  $0_g^-$ , they become comparable to those of the  $0_u^+$  and  $1_g$  states for detunings  $\Delta_p > 1 \text{ cm}^{-1}$ .*

### III. EXCITATION TO $5S+5P_{1/2}$ STATES

The photoassociation of two free atoms to molecular levels of the  $0_u^+$ ,  $1_g$ , and  $0_g^-$  states is first studied. The continuum of scattering states is represented by a finite number of box states [14,15,27]. These box states are normalized to 1. To obtain the energy normalization which is usually employed for continuum states, they have to be weighted by the density of states of the box (see Ref. [15] for details). The initial state of the calculations is chosen to be the  $s$ -wave scattering state with collision energy  $E_{\text{coll}}$  equivalent to a temperature  $T=E_{\text{coll}}/k_B=105 \mu\text{K}$  (with  $k_B$  the Boltzmann constant). Such a state is typical for the conditions in a MOT. At these low temperatures the short-range part of the scattering wave functions is independent of temperature. This means that the positions of the inner nodes of the scattering wave functions approximately match the nodes of the last bound level. If the Franck-Condon radius corresponding to the central frequency of the pulse,  $R_C(\omega_p)$ , is located within this region determined by the extension of the last bound level, the excitation probability is roughly temperature independent. In the following,  $\pi$  polarization of the laser will be assumed and the rotational angular momentum of the molecules is taken to be  $J=0$ .

#### A. Excitation efficiency to the $0_u^+$ , $1_g$ , and $0_g^-$ states

For weak fields, the excitation efficiency is completely determined by the dipole matrix elements and by the detuning and spectral bandwidth of the laser. Figure 3 shows the

TABLE I. Excited-state population after the pulse ( $P_{\text{exc}}$ ) compared to the absolute value squared of the dipole matrix (DPM) elements between the initial state and one exemplary vibrational level (the one which is resonant with the central frequency of the pulse) for transitions from the singlet ground ( $0_u^+$ ) and lowest triplet ( $1_g, 0_g^-$ ) state. The last column lists the population of the last bound *ground* or lower triplet state level, respectively, after the pulse. The pulse energy is 4.2 nJ in all cases, and  $\pi$  polarization has been assumed.

State	$P_{\text{exc}}$	DPM elements ( $E_{v'}=\hbar\Delta_p$ ) <sup>a</sup>	$P_{\text{low,last}}$
$0_u^+$	$2.9 \times 10^{-5}$	$3.5 \times 10^{-5}$	$5.3 \times 10^{-5}$
$1_g$	$3.8 \times 10^{-5}$	$4.7 \times 10^{-5}$	$1.0 \times 10^{-4}$
State	$P_{\text{exc}}$	DPM elements ( $E_{v'}=\hbar\Delta_p$ ) <sup>b</sup>	$P_{\text{low,last}}$
$0_u^+$	$3.1 \times 10^{-5}$	$2.5 \times 10^{-5}$	$5.8 \times 10^{-6}$
$0_g^-$	$2.4 \times 10^{-6}$	$6.8 \times 10^{-6}$	$3.5 \times 10^{-8c}$

<sup>a</sup> $\Delta_p=4.1 \text{ cm}^{-1}$ ,  $\tau_p=10\text{ps}$ .

<sup>b</sup> $\Delta_p=8.6 \text{ cm}^{-1}$ ,  $\tau_p=5 \text{ ps}$ .

<sup>c</sup>For  $0_g^-$  the highest population in a bound level of the lowest triplet state is found for  $v=\text{last } 2$ ,  $P_{g,\text{last}-2}=6.2 \times 10^{-7}$  rather than  $v=\text{last}$ .

absolute value squared of the dipole matrix (DPM) elements  $|\langle \varphi_{v'}^{\text{exc}} | \mu_{\pi}(\hat{\mathbf{R}}) | \varphi_{T=105 \mu\text{K}}^g \rangle|^2$  versus binding energy  $E_{v'}^{\text{exc}}$  or, respectively, the laser detuning, for three different ranges of detunings (exc= $0_u^+, 1_g, 0_g^-$ ). Very close to the atomic resonance ( $\Delta_p < 1 \text{ cm}^{-1}$ , upper panel), the DPM elements for transitions into  $0_g^-$  are about two orders of magnitude smaller than those for transitions into  $0_u^+$  and  $1_g$ . This is due to the  $1/R^6$  nature of  $0_g^-$  at long range as compared to  $1/R^3$  for  $0_u^+$  and  $1_g$ . It is noteworthy that this region of small detunings where PA is most efficient is *unlikely* to be accessible in an experiment with short pulses due to the bandwidth of the pulse. Such pulses contain spectral components corresponding to the atomic resonance, which can destroy the MOT [19,20]. The pulse therefore has to be either far detuned from the atomic line or the resonant spectral components have to be filtered out. This filtering can only be done with a finite spectral resolution which is of the order of  $1 \text{ cm}^{-1}$ . For larger detunings ( $\Delta_p > 1 \text{ cm}^{-1}$ , Fig. 3, middle and lower panel) the DPM elements for all three potentials are of the same order of magnitude. The difference between  $1/R^3$  and  $1/R^6$  potentials lies only in the different density of molecular levels, with that of a  $1/R^6$  potential being significantly smaller. Since for PA with *pulses* more than one level is resonant within the spectral bandwidth, this density of states becomes important for the excitation efficiency. The overall excitation efficiency for PA with short pulses will be smaller than one might initially expect due to the inaccessibility of the range of very small detunings. It has furthermore to be concluded from Fig. 3 that excitation by pulses is unlikely to be selective: Only very few detunings exist where the DPM elements are large for one potential and negligible for the other ones (cf.  $\Delta_p \sim 7.5 \text{ cm}^{-1}$ , Fig. 3, middle panel). In most cases, the bandwidth of the pulse will comprise resonances with significant DPM elements for more than one potential.

Table I presents PA probabilities obtained from solving the time-dependent Schrödinger equation (4) for all three

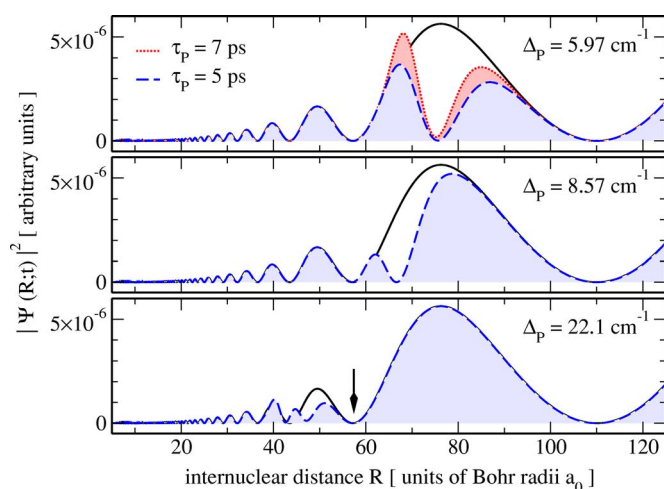


FIG. 4. (Color online) The singlet ground-state wave function (absolute value squared) before (black solid line) and after the pulse (colored dashed and dotted lines). The arrow indicates the position of the last node of the last bound ground-state level. Different detunings and pulse bandwidths are compared: *The spectral width of the pulse determines the size of the photoassociation window while the detuning fixes its position.*

Hamiltonians, Eqs. (1)–(3), and for transform-limited pulses. Due to the normalization of the box state, the PA probability is given by the excited-state population after the pulse,  $P_{\text{exc}}$ . Each of the detunings was chosen to be resonant with levels in both compared potentials. The corresponding DPM elements of the central level is given in the third column of Table I. The PA probabilities for transitions to  $0_u^+$  and  $1_g$  at  $\Delta_p = 4.1 \text{ cm}^{-1}$  are comparable and reflect the DPM elements of the central level. At  $\Delta_p = 8.6 \text{ cm}^{-1}$ , the PA probability for  $0_u^+$  is an order of magnitude larger than for  $0_g^-$ , while the corresponding DPM elements differ only by a factor of 3.7. This reflects the different densities of states in a  $1/R^3$  and a  $1/R^6$  potential. The last column of Table I lists the probability of forming molecules in the last bound level of the singlet ground or lowest triplet state. For small detuning ( $\Delta_p = 4.1 \text{ cm}^{-1}$ ), this probability is even higher than that of creating excited-state molecules, a phenomenon which has already been observed for cesium [14]. For larger detuning ( $\Delta_p = 8.6 \text{ cm}^{-1}$ ), this probability is decreased as compared to  $P_{\text{exc}}$  but is still significant. The explanation of this behavior will be given below.

The PA pulse creates a wave packet composed of a superposition of several vibrational levels with time-dependent coefficients, on the excited electronic state. In addition the PA leaves a corresponding “hole” in the ground-state wave function. This phenomenon is illustrated in Figs. 4 and 5 for excitation from the singlet ground state to  $0_u^+$ . The ground-state components before and after the pulse ( $t = t_p \pm 4\sigma_p$ ) are compared in Fig. 4 for different detunings and pulse durations corresponding to different spectral bandwidths. For  $\Delta_p = 5.97 \text{ cm}^{-1}$ , the Franck-Condon point of the central frequency corresponds to a maximum in amplitude of the ground-state scattering wave function. It also coincides with the outermost maximum of the last bound level. The pulse cuts a hole around the position of this maximum: Population

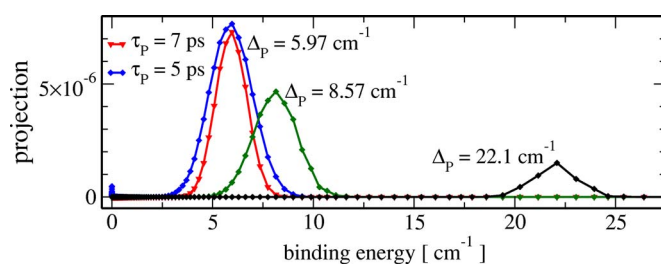


FIG. 5. (Color online) The projection of the excited-state wave function after the pulse onto the  $0_u^+$  excited-state vibrational eigenfunctions (absolute values squared) vs the binding energy of the vibrational levels: *The excited-state vibrational distributions reflect the detuning from the atomic line (peak position) and the spectral width (peak width) of the pulse.*

transfer occurs within the *photoassociation window*, defined by the range of distances given by the Franck-Condon points  $R_C(\omega)$  for all frequencies within the bandwidth of the pulse [14]. The depth of the hole is determined by the intensity or pulse energy. The width of the PA window is given by the spectral bandwidth of the pulse; cf. the blue dashed and red dotted lines in the upper panel of Fig. 4 ( $\Delta\omega_p = 2.94 \text{ cm}^{-1}$  for  $\tau_p = 5 \text{ ps}$ ,  $\Delta\omega_p = 2.10 \text{ cm}^{-1}$  for  $\tau_p = 7 \text{ ps}$ ). Further detuning of the central frequency from the atomic line shifts the PA window to shorter internuclear distances (Fig. 4, middle and lower panels). At these shorter distances, the probability density of the ground-state wave function is significantly smaller, and hence less population can be excited.

Figure 4 explains the relation between the PA detuning and the population of the last bound ground-state level,  $P_{g,\text{last}}$ , for  $0_u^+$ . As reported in Table I,  $P_{g,\text{last}}$  is larger than  $P_{\text{exc}}$  for  $\Delta_p = 4.1 \text{ cm}^{-1}$ , but smaller than  $P_{\text{exc}}$  for  $\Delta_p = 8.6 \text{ cm}^{-1}$ . This is because at  $4.1 \text{ cm}^{-1}$  the center of the PA window is close to the position of the maximum of the ground-state scattering wave function, as seen similarly in the upper panel. Since this position is almost identical with the position of the outermost maximum of the last bound level and since the outermost peak contains about 85% of the probability density of this level, population transfer into this level via Rabi cycling is extremely efficient. At  $8.6 \text{ cm}^{-1}$ , the PA window is moved toward the position of the last node of the last bound level (cf. Fig 4, middle panel), where less population is available to be transferred. In conclusion, the PA pulse is most efficient with respect to both  $P_{\text{exc}}$  and  $P_{g,\text{last}}$  if the Franck-Condon point of its central frequency,  $R_C(\omega_p)$ , corresponds to the position of the last maximum of the last bound level and its spectral bandwidth is large enough such that the PA window comprises this last peak.

Figure 5 displays the projections of the excited-state wave packet generated by the pulse onto the vibrational levels of  $0_u^+$ . The Gaussian peaks reflect the Gaussian shape of the pulse envelope. The peak position is determined by the detuning of the laser, while the peak width mirrors the spectral bandwidth. The height of the peaks is entailed by the DPM elements which decreases for larger detuning from the atomic line (all pulses have the same pulse energy). Note the nonzero values of the projection close to the atomic line for  $\tau_p = 5 \text{ ps}$  and  $\Delta_p = 5.97 \text{ cm}^{-1}$ . Even though the spectral com-

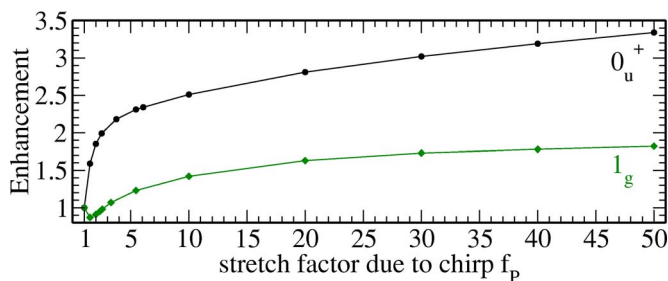


FIG. 6. (Color online) Enhancement—i.e., ratio of excited-state population after a positively chirped pulse to excited-state population after the transform-limited pulse with the same spectral width  $\Delta\omega_p$  vs stretch factor  $f_p$  characterizing the strength of the chirp: A positive frequency chirp leads to more efficient population transfer for transitions to both  $0_u^+$  and  $1_g$  states.

ponents close to  $\Delta_p=0$  are extremely small, the atomic resonance is excited due to its huge DPM elements. This emphasizes the importance of filtering out spectral components around the atomic line.

### B. Positive frequency chirp: Enhanced excitation probability

The next step is to relax the condition of transform-limited Gaussian pulses and to introduce a frequency chirp where the central frequency of the pulse changes linearly with time. Chirped pulses have been introduced in the context of molecular  $\pi$  pulses [37]. The principle underlying this concept is that if the pulse is much shorter than the vibrational period, the nuclear motion is not resolved by the pulse. The molecule can be treated as an effective two-level system, and chirping the pulse enforces the adiabatic following conditions. PA with chirped pulses has been discussed within a Landau-Zener picture. It was found that a positive chirp maximizes population transfer by countering the slope of the excited-state potential [13,16].

The calculations presented in Fig. 6 show the ratio of the excited-state population after a positively chirped pulse to the excited-state population after the corresponding transform-limited pulse for transitions into  $0_u^+$  and  $1_g$ . The pulse has a detuning of  $\Delta_p=4.1$  cm $^{-1}$ , a pulse energy of 4.2 nJ, FWHM of 10 ps, and a corresponding spectral bandwidth of  $\Delta\omega_p=1.47$  cm $^{-1}$ . The difference between these calculations and those of Refs. [13,16] lies in the description of the initial state: For the Gaussian wave packet of Refs. [13,16] complete population inversion to bound excited-state levels can be obtained, while for a scattering state as in Fig. 4 population is transferred only from within the photoassociation window (see Ref. [15] for a detailed discussion). The larger enhancement for  $0_u^+$  than for  $1_g$  is explained by the different topology of the potentials leading to different values  $R_c(\omega_p)$ . For  $\Delta_p=4.1$  cm $^{-1}$ , the center of the PA window is found at  $R_C=86.5$  a.u. for  $0_u^+$ , but at  $R_C=69.9$  a.u. for  $1_g$ —i.e., for  $0_u^+$  it is close to a maximum, while for  $1_g$  it is close to a node of the ground-state wave function (cf. Fig. 4). Therefore within the PA window, less population is available for transfer to  $1_g$  than to  $0_u^+$ . A large amount of this small population is already excited by a transform-limited pulse of 4.2 nJ; thus, chirping cannot increase it further.

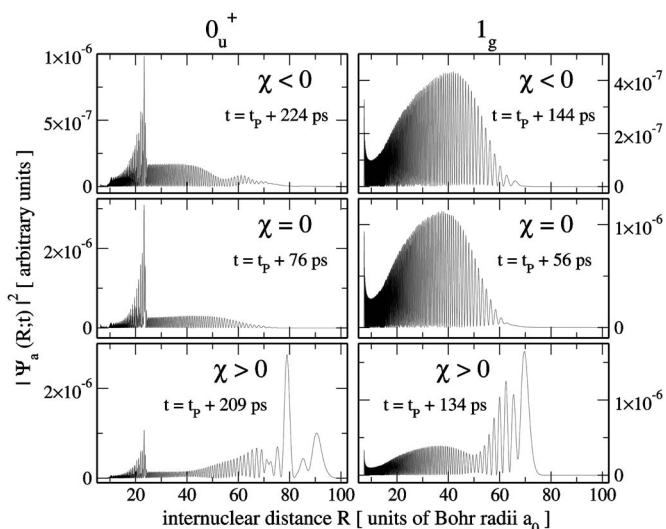


FIG. 7. The best focused wave functions for excitation to  $0_u^+$  (left) and  $1_g$  (right) for transform-limited 10-ps pulses (middle) and negatively (top) and positively (bottom) chirped pulses. The  $A^1\Sigma_u^+$  (left) and  $^3\Pi_g$  (right) components of the excited-state wave functions are shown—i.e., the component of the state which is coupled to the singlet ground and lowest triplet states by the laser light: *The resonant spin-orbit coupling in the  $0_u^+$  states leads to a large population at short distances ( $R\sim 20$  a.u.).*  $t_p$  denotes the maximum of the field amplitude, the stretch factors are  $f_p=6.1$  (left) and  $f_p=5.5$  (right),  $\Delta_p=4.1$  cm $^{-1}$ ,  $\mathcal{E}_p=4.2$  nJ.

### C. Negative frequency chirp: Shaping the excited-state wave packet

When the chirp is negative, large frequencies precede small ones during the pulse. Consequently, the partial wave packets at large distances are excited before the ones at shorter distances. In an eigenstate picture, levels with large vibrational period are excited before those with smaller vibrational period. The chirp can now be chosen to synchronize the excitation of partial wave packets such that they will all arrive at exactly the same time at the inner classical turning point [14,15]. The value of the chirp can be estimated in terms of the vibrational period and the revival period of the level which is resonant with the central frequency of the pulse—i.e., in terms of the vibrational spectrum [15].

Figure 7 shows how a negatively chirped pulse suppresses the dispersion of the wave packet while a positively chirped pulse enhances the dispersion. A similar behavior has been reported for cesium in Refs. [14,15]. The focusing effect for a negative chirp compared to a transform-limited pulse is less pronounced than reported in Refs. [14,15]. This is due to the larger detuning: Close to the dissociation limit, the vibrational periods increase algebraically and more correcting for dispersion is needed. Therefore active shaping of the excited-state wave packet by a negative chirp becomes less crucial with increasing detuning.

A negative chirp compared to a transform-limited pulse can suppress the PA probability. In the range of detunings of a few wave numbers, negative chirp either left the PA probability constant or reduced it by up to a factor of 10. The reduction in PA probability was observed for both  $0_u^+$  and  $1_g$

potentials. This is unlike the case of cesium where a negative chirp led to an increase of the PA probability by a factor of 3 [14].

The resonant spin-orbit coupling in the case of the  $0_u^+$  potentials<sup>1</sup> causes a piling-up of population around  $R=25$  a.u. which corresponds to the outer turning point of the  $0_u^+(P_{3/2})$  potential. It is in line with the shape of the eigenfunctions (cf. the left-hand sides of Figs. 7 and 2). In the case of the  $1_g$  potentials, the maximum of population is found for  $R=40$  a.u. In a pump-dump scheme, a second pulse transfers these wave packets back to the singlet ground or lowest triplet state with the goal of populating deeply bound levels. The positions of the maxima,  $R=25$  a.u. and  $R=40$  a.u., therefore have to be compared to the outer turning point of the bound ground-state levels. Since levels with binding energy larger than one wave number have their outer turning point at distances shorter than  $R=35$  a.u., efficient population transfer into these more deeply bound levels can only be expected for  $0_u^+$ . Levels bound by less than  $1 \text{ cm}^{-1}$  can be efficiently populated by a single PA pulse and therefore do not require a two-color scheme.

Finally, the population  $P_{g,\text{last}}$  of the last bound levels of the singlet ground and lowest triplet states is roughly identical for pulses with the same frequency content; i.e., it is independent of a chirp.

#### IV. DEEXCITATION TO $X^1\Sigma_g^+$ GROUND- AND $a^3\Sigma_u^+$ LOWER-TRIPLET-STATE MOLECULES

In order to obtain stable molecules in the singlet ground or lowest triplet states, a second or dump pulse may be applied to the excited-state wave packet. Some vibrational levels in the  $X^1\Sigma_g^+$  ground and  $a^3\Sigma_u^+$  lower triplet states are already populated by the first pulse. However, these levels are very loosely bound. A dump pulse can be optimized to populate more deeply bound levels. The concepts developed in Ref. [27] will be employed, in particular the time dependence of the DPM elements between the excited-state wave packet and the bound ground- and lowest-triplet-state levels, and the idea of employing a narrow-bandwidth pulse, suitably detuned with respect to the PA pulse, to achieve transfer into a single vibrational level. As was shown in Ref. [27], for weak dump pulses the population transfer to the lowest triplet state is completely determined by the DPM elements and the central frequency and spectral bandwidth of the pulse. The difference between the current study and Ref. [27] is due to the stabilization mechanism allowing for efficient transfer to more deeply bound levels. In the study of cesium, the stabilization mechanism was most efficient for the wave packet localized at the soft repulsive wall of the outer well of the  $0_g^-(P_{3/2})$  state. Presently, for rubidium below the  $D_1$  line, stabilization is afforded by vibrational levels of  $0_u^+(P_{1/2})$

<sup>1</sup>Note that the optimal chirp needs to be estimated from the Hund's-case (a)  $A^1\Sigma_u^+$  potential without spin-orbit coupling. The vibrational spectrum is so strongly perturbed by the resonant coupling that the chirp as a function of binding energy exhibits divergences.

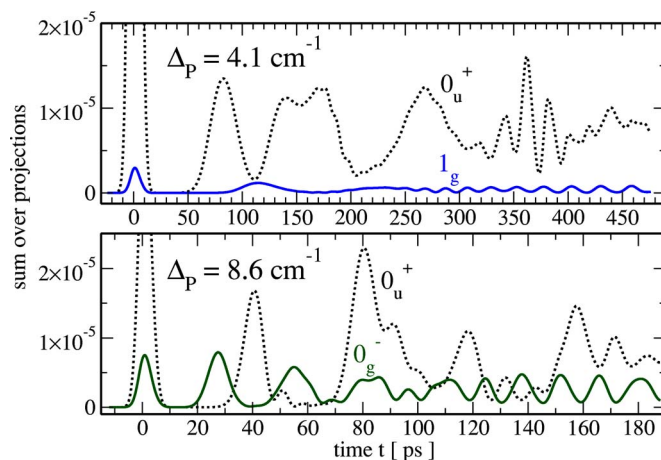


FIG. 8. (Color online) The sum over all projections (absolute values squared) of the excited-state wave packet to bound singlet ground- and lowest-triplet-state levels after excitation to  $0_u^+$  (black dotted lines), to  $1_g$  (blue solid line, top), and to  $0_g^-$  (green solid line, bottom): *Deexcitation into bound levels is far more efficient from the  $0_u^+$  state than from  $1_g$  or  $0_g^-$ .* The transform-limited excitation pulses have  $\tau_p=10$  ps (top) and  $\tau_p=5$  ps (bottom) and pulse energy of 4.2 nJ.

which are in resonance with a level of  $0_u^+(P_{3/2})$ .

Since coherent effects between the pump and dump pulses are neglected, the excited-state population after the PA pulse can be normalized to 1. Populations correspond then directly to probabilities. Figure 8 shows the sum over the DPM elements between the excited-state wave packet  $\Psi_e(t)$  and all bound singlet ground- and lowest-triplet-state levels,  $\sum_{v''} |\langle \varphi_{v''}^g | \mu_\pi(\hat{\mathbf{R}}) | \Psi_e(t) \rangle|^2$  for  $0_u^+$ ,  $1_g$ , and  $0_g^-$  [ $e$  denotes the channel which is coupled by the laser field to the singlet ground or lowest triplet state in Eqs. (1)–(3)—i.e.,  $A^1\Sigma_u^+$  and  $3\Sigma_u^+$ ]. The sum over projections is compared for  $0_u^+$  and  $1_g$  at a PA pulse detuning of  $\Delta_p=4.1 \text{ cm}^{-1}$  and for  $0_u^+$  and  $0_g^-$  at  $\Delta_p=8.6 \text{ cm}^{-1}$ . The origin of time is set equal to the time when the amplitude of the PA pulse is maximum,  $t_p=0$ . The sum over projections shows oscillations which reflect the excited-state wave packet dynamics. At later times, the oscillations are washed out due to wave packet dispersion (the excitation pulses are transform limited). At both detunings, the projections are larger for  $0_u^+$  than for  $1_g$  and  $0_g^-$ , respectively; i.e., stabilization is expected to be most efficient for  $0_u^+$ .

The sum over the DPM elements does not reveal which levels in the singlet ground and lowest triplet states are accessible by the dump pulse. Figure 9 therefore shows the DPM elements  $|\langle \varphi_{v''}^g | \mu_\pi(\hat{\mathbf{R}}) | \Psi_e(t) \rangle|^2$  as a function of time and binding energy  $E_{v''}$  of the singlet ground- and lowest-triplet-state levels  $v''$  (same parameters as in Fig. 8). For both  $1_g$  and  $0_g^-$  states, deexcitation can transfer population only into the last two to three levels of the lowest triplet state [Figs. 9(b) and 9(d)]. These levels are bound by less than  $0.1 \text{ cm}^{-1}$ , and they are already populated efficiently by the PA pulse (cf. Table I). In contrast, for  $0_u^+$  DPM elements with both the last three and more deeply bound levels are significant. The levels which are bound by  $10\text{--}4 \text{ cm}^{-1}$  have vibrational index

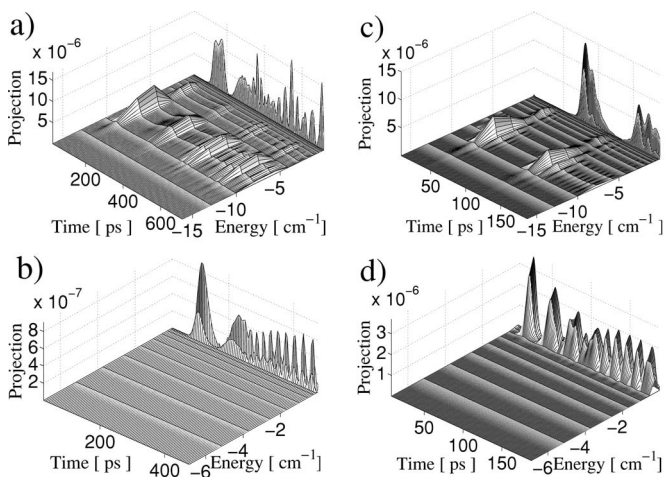


FIG. 9. The projections (absolute values squared) of the excited-state wave packet to all bound singlet ground- and lowest-triplet-state levels vs time and binding energy after excitation to  $0_u^+$  (a), (c),  $1_g$  (b), and  $0_g^-$  (d) [(a), (b)  $\Delta\omega_p=4.1\text{ cm}^{-1}$ , (c), (d)  $\Delta\omega_p=8.6\text{ cm}^{-1}$ ]: *Deexcitation from the  $1_g$  and  $0_g^-$  states can populate only the last bound levels, while  $0_u^+$  allows for transitions into more deeply bound ground-state levels.*

$v''=109-112$  (the last bound level has  $v''=120$ ). The outer classical turning points of the corresponding wave functions are located between  $R\sim 24$  a.u. and  $R\sim 28$  a.u. (as compared to  $R\sim 170$  a.u. for the last bound level); i.e., their outermost maximum is located at about the same position as the peak in the excited-state wave packets in the left-hand side of Fig. 7. It can therefore be concluded that the resonant spin-orbit coupling in the  $0_u^+$  states provides the stabilization mechanism into more deeply bound ground-state levels. It is obvious from Figs. 9(a) and 9(c) that the vibrational period of the excited-state wave packet as well as its compactness is determined by the detuning as expected.

The DPM elements of the  $0_u^+$  ( $A^1\Sigma_u^+$ ) excited-state wave packet after excitation with chirped PA pulses is shown in Fig. 10. A negative frequency chirp of the excitation pulse leads to a compact wave packet oscillating in the excited-state potential. These oscillations are reflected in the clearly separated peaks of the projections [Fig. 10(a)]. After a posi-

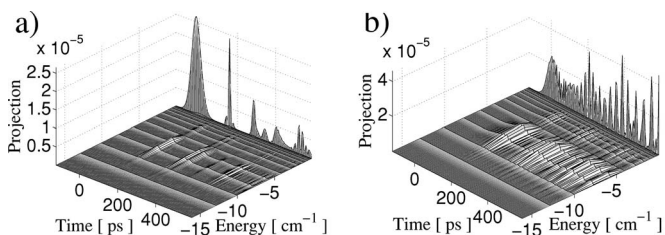


FIG. 10. The projections (absolute values squared) of the excited-state wave packet to all bound ground-state levels vs time and binding energy after excitation by negatively (a) and positively (b) chirped pulses to  $0_u^+$  [ $f_p=6.1$ ; cf. the left-hand side of Fig. 7 for examples of the excited-state wave packets and Fig. 9(a) for the projections of the corresponding transform-limited case]: *Deexcitation into more deeply bound ground-state levels is possible after transform-limited as well as after chirped pump pulses.*

tively chirped excitation pulse the wave packet is spread out in coordinate space and the peaks of the projections are smeared out [Fig. 10(b)]. Since chirping does not affect the spectral bandwidth of the pulse, the excited-state wave packets after chirped and after transform-limited pulses are composed of the same vibrational levels. Hence the ground-state levels which are accessible by a second pulse are identical [cf. Figs. 10 and 9(a)].

The outcome of the calculations with a second or dump pulse are now presented. The goal is to transfer as much of the excited-state wave packet as possible into a single, more deeply bound ground-state level. Calculations have therefore been done only for the  $0_u^+$  states. The initial state of the example presented in the following is given by the excited-state wave packet after excitation by a PA pulse with  $\Delta_p=4.1\text{ cm}^{-1}$  and  $\tau_p=10\text{ ps}$  (cf. left-hand side of Fig. 7). The time delay between PA and stabilization pulses which best achieves the goal can be read off the time-dependent DPM elements (cf. Figs. 9 and 10—for example,  $t_D-t_p=81.5\text{ ps}$  after the transform-limited PA pulse). The spectral bandwidth of the dump pulse is determined by the requirement of populating a single vibrational level, chosen to be  $v''=111$ .  $\Delta_D$  needs to be smaller than the vibrational-level spacing which is approximately  $1.7\text{ cm}^{-1}$  for this level. This corresponds to dump pulses with FWHM  $\tau_D\geq 8\text{ ps}$ . The detuning is chosen such that the energies of the excited-state wave packet and the target level are brought into resonance,  $\Delta_D=-1.64\text{ cm}^{-1}$  for  $v''=111$ ; i.e., the dump pulse is blue detuned with respect to the  $D_1$  line. The ground-state population  $P_g=|\langle g|\Psi(t)\rangle|^2$  and the population of bound ground-state levels,  $P_{\text{bound}}=\sum_{v''}\langle\varphi_{v''}^g|\Psi(t)\rangle|^2$ , after a dump pulse of  $\tau_D=10\text{ ps}$  are shown in Fig. 11(a) as a function of pulse energy. Since the narrow-bandwidth dump pulses are resonant only with bound ground-state levels and not with the ground-state continuum,  $P_g$  and  $P_{\text{bound}}$  are basically identical. The calculations of Fig. 11(a) start from three different initial states: the excited wave packet after a 10-ps transform-limited PA pulse (dotted lines) as well as after the corresponding positively and negatively chirped PA pulses [dashed and solid lines, respectively; cf. Figs. 9(a) and 10]. The highest ground-state population is achieved after a transform-limited PA pulse. The positively chirped PA pulse provides the least effective starting point for stabilization. This is due to the large wave packet dispersion. Generally, the achieved ground-state population is much higher than expected from the DPM elements: Up to 50% of the excited-state wave packet can be transferred to the ground state. The vibrational distribution of the final ground-state wave packet,  $|\langle\varphi_{v''}^g|\Psi_g(t)\rangle|^2$ , shown in Fig. 11(c), demonstrates that as intended this population ends up almost exclusively in a single vibrational level: namely,  $v''=111$  bound by  $5.74\text{ cm}^{-1}$ . An example of a ground-state wave packet after the dump pulse is shown in Fig. 11(b) which confirms the pure eigenstate nature of  $\Psi_g(R;t)$ . The enhanced population transfer by the stabilization pulse is attributed to a dynamical effect due to spin-orbit coupling: The excited-state wave packet has components on both  $A^1\Sigma_u^+$  and  $b^3\Pi_u$  states, but only the  $A^1\Sigma_u^+$  component is coupled to the ground state by the field. When the dump pulse acts, the  $A^1\Sigma_u^+$  component is depleted by the pulse, but “refilled” by

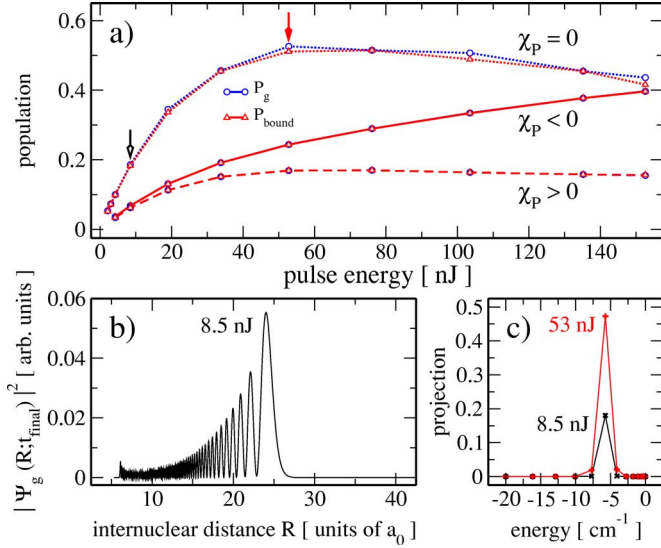


FIG. 11. (Color online) (a) Ground-state population  $P_g$  (blue circles) and population of bound ground-state levels  $P_{\text{bound}}$  (red triangles) after a transform-limited dump pulse with FWHM of 10 ps (solid lines) following excitation by a transform-limited (dotted lines), a negatively (solid lines), and a positively (dashed lines) chirped pump pulse. (b) The final ground-state wave packet after a dump pulse with an energy of 8.5 nJ [corresponding to the black arrow in (a)]. (c) The projection of the final ground-state wave packet onto vibrational levels (absolute values squared)—i.e., the vibrational distribution vs binding energy after dump pulses with pulse energies of 8.5 nJ and 53 nJ [corresponding to the black and red arrows in (a)]. Up to 50% of the excited-state wave packet can be transferred to a single, more deeply bound ground-state level.

the resonant spin-orbit coupling. Thus significantly more population is channeled to the ground state than expected from the DPM elements which only contain the  $A^1\Sigma_u^+$  component. This effect is most pronounced when the wave packet is focused around the spin-orbit peak (cf. Fig. 7, left-hand side) and therefore works best after transform-limited or negatively chirped PA pulses.

Transform-limited dump pulses with a FWHM of 5 ps give similar results with slightly broader vibrational distributions. Chirping the dump pulses decreases the population transfer into more deeply bound levels: The chirp stretches the pulses such that the duration becomes much larger than the time in which the wave packet stays at short distances.

## V. SENSITIVITY ON THE DESCRIPTION OF THE SPIN-ORBIT COUPLING

The spin-orbit coupling having resonant character for the  $0_u^+$  states provides a mechanism for the formation of ground-state molecules bound by a few wave numbers. The extent to which the dump step depends on the specific model of the spin-orbit coupling (SOC) is explored. Two model curves [38,39] to describe the  $R$  dependence of the SOC are employed. At this time, no *ab initio* or spectroscopic data allowing for a more accurate description are available. The first model curve  $W_1(R)$  has been obtained from *ab initio* calculations of the  $R$ -dependent SOC of  $\text{Cs}_2$  [40] and scaling with

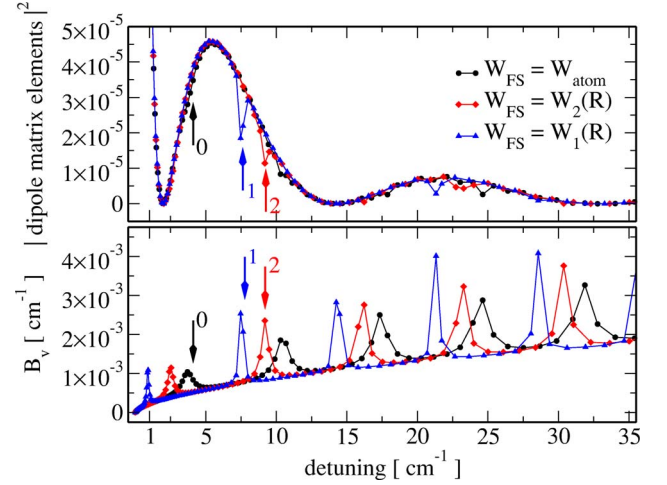


FIG. 12. (Color online) The absolute values squared of the dipole matrix elements  $|\langle \varphi_{v'}^{\text{exc}} | \mu_{\pi}(\hat{\mathbf{R}}) | \varphi_{T=105}^g \mu_K \rangle|^2$  (top) and the rotational constants  $B_{v'} = \langle 1 / (2\mu \hat{\mathbf{R}}^2) \rangle$  of the  $0_u^+$  excited states (bottom) for three different models of the spin-orbit coupling. The peaks of the rotational constants correspond to levels which are strongly perturbed by the resonant coupling. The specific model of the spin-orbit coupling has almost no influence on the dipole matrix elements. It does affect the position of the strongly perturbed levels which are crucial for deexcitation toward more deeply bound ground-state molecules. Therefore the excitation probability is expected to be roughly independent of the description of the spin-orbit coupling. However, in order to assure an efficient dump step, the pump detuning needs to be adjusted such that resonant excited-state levels are populated.

the ratio of the fine structure splittings  $\Delta E_{\text{FS}}$  of rubidium and cesium [39].  $W_1(R)$  displays a minimum at  $R \approx 11$  a.u., and at the crossing point of the potentials (at  $R \approx 9.5$  a.u.), the SOC is reduced to about 65% of its asymptotic value. It was argued in Ref. [39] that the reduction of the coupling at the crossing point is probably overestimated in  $W_1(R)$ . Therefore a second model curve  $W_2(R)$  was introduced showing a similar dependence on  $R$  as  $W_1(R)$  but with the coupling at the crossing point reduced to only 80% of the asymptotic value. The  $R$  dependence of both functions  $W_1(R)$  and  $W_2(R)$  is displayed in Fig. 2 of Ref. [39]. At long range, both curves become constant and equal the atomic value.

In the following, the results of Secs. III and IV for  $W_{\text{SO}} = \text{const}$  are compared to those obtained with  $W_{\text{SO}} = W_1(R)$  and  $W_{\text{SO}} = W_2(R)$  for transitions via  $0_u^+$ . The binding energies of the excited-state levels are slightly shifted for  $W_1(R)$  and  $W_2(R)$  as compared to constant coupling. These shifts are negligible with respect to the bandwidth of the pulse. The excitation probability is determined by the dipole matrix elements between the initial scattering state and bound vibrational levels of the  $0_u^+$  excited states. The absolute values squared of the dipole matrix elements are shown in the upper panel of Fig. 12 for the three different SOC models. Except for single levels where the wave function is strongly modified by the coupling, the DPM elements are almost identical. This is to be expected because the overlap between the scattering state and the excited-state levels is biggest at large distances  $R$  where all three SOC are constant. For the levels

TABLE II. Excited-state population after the PA pulse ( $P_{\text{exc}}$ ) for transitions to  $0_u^+$  and three different models of the spin-orbit coupling,  $W_{\text{SO}}$ . Also listed are the absolute values squared of the dipole matrix (DPM) elements between the initial state and the vibrational level resonant with the central frequency and the population of the last bound *ground-state* level after the pulse. The employed detunings are indicated by arrows in Fig. 12. The pulse energy is 4.2 nJ in all cases, and  $\pi$  polarization has been assumed.

$\Delta_p$ [ $\text{cm}^{-1}$ ]	$W_{\text{SO}}$	$\tau_p$ [ps]	$P_{\text{exc}}$	DPM elements ( $E_{v'} = \hbar \Delta_p$ )	$P_{g,\text{last}}$
4.1	const	10	$2.9 \times 10^{-5}$	$3.5 \times 10^{-5}$	$5.3 \times 10^{-5}$
4.1	$W_1(R)$	10	$2.9 \times 10^{-5}$	$3.9 \times 10^{-5}$	$5.3 \times 10^{-5}$
7.6	$W_1(R)$	10	$1.6 \times 10^{-5}$	$2.2 \times 10^{-5}$	$9.2 \times 10^{-6}$
7.6	$W_1(R)$	5	$4.6 \times 10^{-5}$	$2.2 \times 10^{-5}$	$9.2 \times 10^{-6}$
9.2	$W_2(R)$	10	$9.2 \times 10^{-6}$	$1.1 \times 10^{-5}$	$4.2 \times 10^{-6}$
9.2	$W_2(R)$	5	$2.4 \times 10^{-5}$	$1.1 \times 10^{-5}$	$4.2 \times 10^{-6}$

where the DPM elements are visibly influenced, the value is reduced by a factor of  $\geq 0.5$ . The overall excitation probability should therefore not significantly depend on the specific model of the SOC. This is confirmed by inspection of the excited-state populations after the PA pulse,  $P_{\text{exc}}$ , listed in Table II.

For deexcitation to more deeply bound molecular levels by the second pulse, it is important for the PA pulse to excite  $0_u^+$  vibrational levels which are strongly perturbed. The resonant or nonresonant character of the excited-state wave functions depends rather sensitively on the model of SOC. Recalling Fig. 2, this is not surprising since the resonant character is caused by the coupling at shorter distances [the outer turning point of  $0_u^+(P_{3/2})$  is  $R \approx 20$  for binding energies of a few  $\text{cm}^{-1}$ ] where  $W_1(R)$  and  $W_2(R)$  differ from  $W_{\text{SO}} = \text{const}$ . Perturbed and regular vibrational levels can be differentiated by their rotational constants  $B_{v'} = \langle 1/(2\mu\hat{R}) \rangle$  as discussed in detail in Refs. [30,38]. The rotational constants for the three different SOC are therefore compared in the lower panel of Fig. 12. The peaks which are superimposed on the smooth dependence of the  $B_{v'}$  on binding energy (or detuning) indicate the strongly perturbed levels. For the initial detuning of  $4.1 \text{ cm}^{-1}$  (arrow labeled 0 in Fig. 12) and a bandwidth of a picosecond pulse, perturbed levels are excited only for constant SOC. In case of the  $R$ -dependent coupling of  $W_1(R)$  and  $W_2(R)$ , regular vibrational levels similar to those of the right-hand side of Fig. 2 are populated (see also Figs. 10 and 11 of Ref. [30]). In that case, it is expected that *no* deeply bound ground-state molecules can be created by applying the second (dump) pulse. In order to investigate whether formation of more deeply bound ground-state molecules is possible at all in case of  $R$ -dependent SOC, the detuning of the pump pulse has been adjusted such that resonant levels are excited (arrows labeled 1 and 2 in Fig. 12; cf. also Table II). For larger detuning ( $7.6 \text{ cm}^{-1}$  and  $9.2 \text{ cm}^{-1}$  as compared to  $4.1 \text{ cm}^{-1}$ ), the vibrational spacing becomes larger. A smaller number of vibrational levels is then resonant within the bandwidth of the PA pulse (for  $\tau_p = 10$  ps,  $\sim 10$  levels as compared to  $\sim 20$  at  $\Delta_p = 4.1 \text{ cm}^{-1}$ ). On the

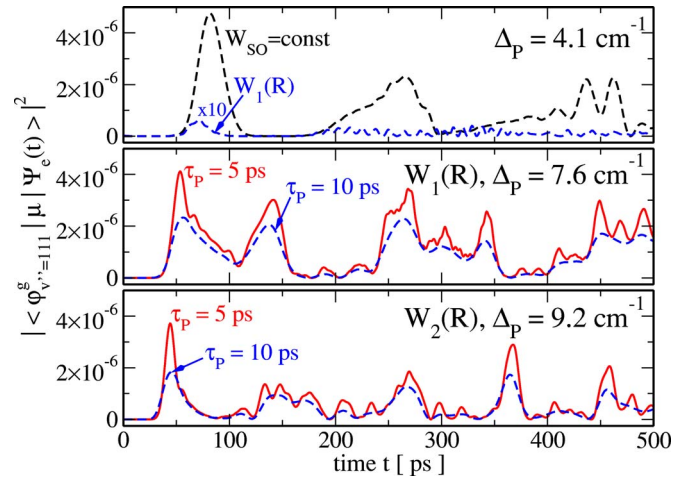


FIG. 13. (Color online) Projection of the time-dependent excited-state wave packet onto the ground-state level  $v''=111$  for three different models of the spin-orbit coupling. The pump pulses are the same as in Table II with the detunings indicated in Fig. 12. In the calculations with  $R$ -dependent spin-orbit coupling, nonresonant excited-state levels are populated in the upper panel while strongly perturbed levels are excited in the middle and bottom panels. Only after excitation of strongly perturbed levels is an appreciable probability for transfer to more deeply bound ground-state levels obtained.

other hand, the main reason for choosing a narrow-bandwidth pulse of  $\tau_p = 10$  ps was to avoid excitation of the atomic resonance. This becomes less likely for larger detuning even if the bandwidth of the pulse is increased. Therefore, calculations for  $\tau_p = 10$  ps are compared to  $\tau_p = 5$  ps in Table II. Both pulses have the same pulse energy of 4.2 nJ. The larger number of vibrational levels resonant within the bandwidth of the pulse for 5 ps compared to 10 ps leads to a higher excitation probability. As in Sec. III (cf. Table I), the excitation probabilities reflect the DPM elements. The probability to populate the last bound level of the *ground state* decreases with increasing detuning (cf. explanation in Sec. III A).

Figure 13 shows the projection of the time-dependent excited-state wave packet onto the ground-state level  $v'' = 111$ ,  $P_{v''=111} = |\langle \varphi_{v''=111}^g | \mu_\pi(\hat{\mathbf{R}}) | \Psi_e(t) \rangle|^2$ , for the different SOC models and different pump detunings [ $E_{\text{bind}}^{v''=111} = 5.74 \text{ cm}^{-1}$ ; cf. Figs. 9(a) and 9(c)]. The upper panel confirms that more deeply bound ground-state levels can only be populated if resonant levels are excited in  $0_u^+$ . The maximum value of  $P_{v''=111}$  is 2 orders of magnitude smaller for  $W_1(R)$  than for  $W_{\text{SO}} = \text{const}$ . However, if the pump detuning is adjusted such as to excite resonant levels, a similar probability to populate more deeply bound levels is observed for  $W_1(R)$  and  $W_2(R)$  as for  $W_{\text{SO}} = \text{const}$  (cf. the maxima of  $P_{v''=111}$  in all three panels). Note that for larger detuning, the best overlap of the excited-state wave packet is obtained for  $v'' = 110$  instead of  $v'' = 111$ . The corresponding binding energy is  $E_{\text{bind}}^{v''=110} = 7.72 \text{ cm}^{-1}$ . Therefore the resulting dump detuning to populate this level,  $\Delta_D = \Delta_p - E_{\text{bind}}^{v''=110}$ , is very small for  $\Delta_p = 7.6 \text{ cm}^{-1}$  and  $9.2 \text{ cm}^{-1}$ . In order to avoid excitation of the

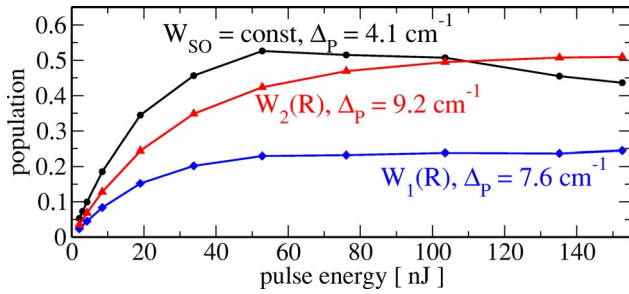


FIG. 14. (Color online) Ground-state population  $P_g$  after 10-ps dump pulses resonant with  $v''=111$  for three different models of the spin-orbit coupling  $W_{SO}$  ( $\tau_p=10$  ps for  $\Delta_p=4.1$  cm<sup>-1</sup>,  $\tau_p=5$  ps for  $\Delta_p=7.6$  cm<sup>-1</sup> and  $9.2$  cm<sup>-1</sup>). The specific model of spin-orbit coupling influences the exact amount of population which can be transferred to more deeply bound levels. However, the scheme is robust and efficient over a large range of pulse energies for all  $W_{SO}$ .

atomic resonance by the dump pulse,  $v''=111$  was chosen as target level instead of  $v''=110$ .

Figure 14 reports the results of time-dependent calculations for the deexcitation step. The pump-dump delay is chosen to correspond to the first maxima in Fig. 13 [ $W_{SO}=\text{const}$  with  $\tau_p=10$  ps, upper panel,  $W_1(R)$  and  $W_2(R)$  with  $\tau_p=5$  ps, middle and lower panel]. The ground-state population after the second (dump) pulse is reduced for  $W_1(R)$  and  $W_2(R)$  as compared to constant SOC. However, the amount of excited-state population which can be transferred to  $v''=111$  of the ground state easily reaches 20% for reasonable pulse energies for all three coupling models. Furthermore, a saturation of the transfer probability as a function of pulse energy is observed for  $R$  dependent SOC. This implies that the dump step is very robust with respect to intensity fluctuations of the field and uncertainties of the model.

## VI. CONCLUSIONS

Pump-dump photoassociation for rubidium-87 below the  $D_1$  line has been analyzed with an emphasis on experimental feasibility. In particular, a setup such as in Refs. [19,20] was considered. All potentials into which population can be excited by a laser field were included in the model. Both potentials and transition dipole moments were based on *ab initio* data and accurate long-range expansions.

The first experiments on ultracold molecule formation with short laser pulses [19,20] did not achieve the goal of creating molecules from atoms in a MOT. Therefore, both pump and dump steps must each be optimized in order to produce stable molecules in their singlet ground or lowest triplet state. For the PA step, an efficient excitation mechanism is provided by the long-range  $1/R^3$  nature of several excited-state potentials. However, the pump pulse is less efficient than one might initially expect from experiments with cw lasers since a rather large detuning from the atomic resonance is required for pulsed lasers. This is due to the pulse bandwidth and the constraint of not exciting the atomic resonance. The best compromise for pump pulses derived from femtosecond oscillators is then found for pulse durations (FWHM) of 5–10 ps and detunings of a few wave numbers.

The bandwidth  $\Delta\omega_p$  of the pump pulse leads to the concept of a photoassociation window which is comprised of the Franck-Condon points corresponding to all resonant frequencies contained in  $\Delta\omega_p$  [14]. The excitation is optimal if the photoassociation window covers the range of internuclear distances of the last maximum of the last bound level of the singlet ground and lowest triplet states. The Franck-Condon radius corresponding to the central frequency (or detuning) of the pump pulse  $R_C(\Delta_p)$  should then be close to the location  $R_{\text{max}}$  of the last maximum of  $\varphi_{v=\text{last}}^g(R)$ . This is the case for pump pulse detunings of a few wave numbers. If one is interested only in exciting atoms, pulses with positive frequency chirp perform best. For subsequent formation of more deeply bound molecules in their singlet ground or lowest triplet state, a pump-dump scheme is required where the optimal first pulse is transform limited. If the detuning from the atomic line is small enough, the PA pulse transfers population also to the last bound levels of the singlet ground or lowest triplet state, respectively. This has already been observed in the case of cesium [14]. The creation of these extremely weakly bound molecules therefore does not require a two-color pump-dump scheme.

The use of two pulses can create molecules in their singlet ground or lowest triplet state (bound by a few wave numbers) provided that an efficient stabilization mechanism exists. For the  $\text{Rb}_2$  states correlated to the  $5S+5P_{1/2}$  asymptote, such a mechanism was identified for  $0_u^+$ , leading to molecules in the  $X^1\Sigma_g^+$  ground state. A pump-dump scheme of photoassociation below the  $D_1$  line via the  $0_u^+$  excited state provides then an efficient means to create ground-state molecules bound by a few wave numbers. In contrast, photoassociation via the  $1_g$  and  $0_g^-$  states will yield molecules in the lower triplet state which are extremely weakly bound. The excitation step from two atoms to the  $0_u^+$  or  $1_g$  and  $0_g^-$  excited states is unlikely to be selective. The efficient stabilization mechanism for  $0_u^+$  has been identified as resonant spin-orbit coupling [31,41]. In a time-dependent process, resonant coupling leads to a dynamical enhancement of stabilization, making the dump step even more efficient than deexcitation to  $\text{Cs}_2$  lower-triplet-state molecules from  $0_g^-(P_{3/2})$ . Depending on the exact description of the spin-orbit coupling, between 20% and 50% of the  $^{87}\text{Rb}_2$   $0_u^+$  excited-state wave packet can be transferred to a single vibrational ground state level as compared to 14% for  $\text{Cs}_2$   $0_g^-(P_{3/2})$  [27]. In order to populate a single ground-state level, dump pulses should have a duration of 10 ps and be blue detuned with respect to the atomic resonance. The creation of a coherent superposition of ground-state levels is also possible. This requires a broader bandwidth—i.e., shorter duration of the dump pulses [27]. However, care must then be taken to avoid excitation of the atomic resonance.

The  $0_u^+$  excited states contain both regular and strongly perturbed levels. It was shown that the excitation of strongly perturbed levels by the pump pulse is essential for deexcitation into more deeply bound ground-state levels. The position of the resonant levels in the vibrational spectrum of  $0_u^+$  and hence the required pump detuning depends rather sensitively on the description of the  $R$ -dependence of the spin-orbit coupling. Within our model, the position of these levels

cannot be predicted accurately. However, the resonant levels are easily identified experimentally by perturbations in the level spacings or rotational constants; see, e.g., Refs. [42,43]. Accurate spectroscopy of the  $0_u^+$  states would improve both the potentials and spin-orbit coupling and allow for obtaining a pump pulse from theory whose central frequency is at resonance with a strongly perturbed level.

The current work has been confined to study molecule formation via excited states correlated to the  $5S+5P_{1/2}$  asymptote. Some conclusions can also be drawn with respect to the  $5S+5P_{3/2}$  asymptote—i.e., the  $D_2$  line. In that case, four attractive potentials into which transitions can be induced by the laser field exist:  $0_g^-$ ,  $1_g$ ,  $0_u^+$ , and  $1_u$ . All four potentials scale as  $1/R^3$  at long range, providing an efficient PA mechanism.  $0_g^-(P_{3/2})$  is known from PA with a cw laser [44] to provide an efficient stabilization mechanism due to the soft repulsive wall of the long-range well. However, a technical difficulty might prevent this route from being feasible: The depth of the  $0_g^-(P_{3/2})$  well is only about  $28\text{ cm}^{-1}$ , and pulse shaping over such a small frequency range is hampered by the spectral resolution of the pulse shaper.

An alternative route to ground-state molecule formation might be provided by employing a femtosecond-frequency comb [45] which can be operated in the picosecond to nanosecond regime. This would avoid the problem of exciting the atomic resonance due to large pulse bandwidth and allow for smaller detunings to be used. The pump step could thus be significantly enhanced, recovering the efficiency of PA with a cw laser.

In the present study, pump-dump photoassociation has been discussed in the frame of a two-atom picture, with zero angular momentum and no transfer of angular momentum from the light to the molecule. One pair of pulses for excitation and stabilization was considered. The calculation of absolute molecule formation rates is beyond the scope of the present study. Such knowledge is important to estimate the laser intensity required to produce a detectable number of ground-state molecules. In order to estimate absolute rates, two questions need to be addressed: (i) averaging over thermal (translational and rotational) and angular distributions of the  $N$ -atom system and (ii) the problem of the repetition rate. Answering the first question requires the solution of the pump-dump dynamics for several initial scattering states (including higher collisional angular momentum than  $l=0$ ) and weighting the results with the Boltzmann factors and the angles between the molecular and polarization axes. The problem of the repetition rate stands for the fact that the second pair of pump and dump pulses will act on a different initial state than the first pair. In particular, the ground-state population within the resonance window might be decreased.

It furthermore has to be ensured that the second pair of pulses does not destroy the molecules created by the first pair. In order to address these questions, the dynamics between the pulse pairs has to be solved. These questions constitute the subject of ongoing work.

In view of prospective applications, vibrationally excited ultracold molecules are not adequate. The next goal is therefore to create ultracold molecules in their absolute rovibronic ground state. Molecules at temperatures below 1 mK are obtained by assembling them from ultracold atoms due to interaction with an external field. The molecule formation process is coherent for magnetic [5–7] or optical [46] Feshbach resonances and for photoassociation with short laser pulses. Feshbach resonances and photoassociation with a single pulse lead to molecules in one of the last bound ground-state levels, just below the dissociation limit. Such molecules typically have bond lengths on the order of  $100a_0$  and are bound by less than  $0.1\text{ cm}^{-1}$ . At these tiny binding energies, singlet and triplet in character, are mixed due to hyperfine interactions. Two-color pump-dump photoassociation allows for creating molecules which are more deeply bound. Bond lengths of  $25a_0$  ( $15a_0$ ) and binding energies of  $5\text{--}10\text{ cm}^{-1}$  ( $110\text{ cm}^{-1}$ ) were found for rubidium (cesium [27]). For subsequent Raman-type transitions to  $v=0$ , molecules with bond lengths of  $(15\text{--}25)a_0$  provide a much better starting point than the very extended Feshbach molecules: Due to better Franck-Condon overlaps, a smaller number of Raman steps and a reduced pulse energy will be required [47]. The advantage of the  $0_u^+$  route as shown in this study for rubidium and of resonant spin-orbit coupling in general [8] is that molecules in their singlet—i.e., their absolute electronic ground state—are created. Therefore a two-color pump-dump scheme with picosecond pulses provides an efficient first step toward obtaining ultracold molecules in their absolute ground state.

#### ACKNOWLEDGMENTS

We are grateful to Mireille Aymar and Olivier Dulieu for making the *ab initio* data of the  $\text{Rb}_2$  potentials and transition dipole moments available to us, to Eliane Luc-Koenig for encouragement and very fruitful discussions, and to Roland Wester for his comments on the manuscript. C.P.K. would like to thank Sandy Ruhman for enlightening discussions on femtosecond laser technology and acknowledges financial support from the Deutsche Forschungsgemeinschaft. This work has been supported by the European Commission in the frame of the Cold Molecule Research Training Network under Contract No. HPRN-CT-2002-00290. The Fritz Haber Center is supported by the Minerva Gesellschaft für die Forschung GmbH München, Germany.

- 
- [1] S. Jochim, M. Bartenstein, A. Altmeyer, G. Hendl, S. Riedl, C. Chin, J. Hecker Denschlag, and R. Grimm, *Science* **302**, 2101 (2003).  
 [2] M. Greiner, C. A. Regal, and D. S. Jin, *Nature (London)* **426**,

537 (2003).

- [3] M. W. Zwierlein, C. A. Stan, C. H. Schunck, S. M. F. Raupach, S. Gupta, Z. Hadzibabic, and W. Ketterle, *Phys. Rev. Lett.* **91**, 250401 (2003).

- [4] J. Doyle, B. Friedrich, R. V. Krems, and F. Masnou-Seeuws, *Eur. Phys. J. D* **31**, 149 (2004).
- [5] K. E. Strecker, G. B. Partridge, and R. G. Hulet, *Phys. Rev. Lett.* **91**, 080406 (2003).
- [6] K. Xu, T. Mukaiyama, J. R. Abo-Shaeer, J. K. Chin, D. E. Miller, and W. Ketterle, *Phys. Rev. Lett.* **91**, 210402 (2003).
- [7] J. Herbig, T. Kraemer, M. Mark, T. Weber, C. Chin, H.-C. Nägerl, and R. Grimm, *Science* **301**, 1510 (2003).
- [8] J. M. Sage, S. Sainis, T. Bergeman, and D. DeMille, *Phys. Rev. Lett.* **94**, 203001 (2005).
- [9] T. Rom, T. Best, O. Mandel, A. Widera, M. Greiner, T. W. Hänsch, and I. Bloch, *Phys. Rev. Lett.* **93**, 073002 (2004).
- [10] C. McKenzie, J. Hecker Denschlag, H. Häffner, A. Browaeys, L. E. E. de Araujo, F. K. Fatemi, K. M. Jones, J. E. Simsarian, D. Cho, A. Simoni, E. Tiesinga, P. S. Julienne, K. Helmerson, P. D. Lett, R. L. Rolston, and W. D. Phillips, *Phys. Rev. Lett.* **88**, 120403 (2002).
- [11] S. D. Gensemer and P. L. Gould, *Phys. Rev. Lett.* **80**, 936 (1998).
- [12] F. Fatemi, K. M. Jones, H. Wang, I. Walmsley, and P. D. Lett, *Phys. Rev. A* **64**, 033421 (2001).
- [13] J. Vala, O. Dulieu, F. Masnou-Seeuws, P. Pillet, and R. Kosloff, *Phys. Rev. A* **63**, 013412 (2000).
- [14] E. Luc-Koenig, R. Kosloff, F. Masnou-Seeuws, and M. Vatasescu, *Phys. Rev. A* **70**, 033414 (2004).
- [15] E. Luc-Koenig, F. Masnou-Seeuws, and M. Vatasescu, *Eur. Phys. J. D* **31**, 239 (2004).
- [16] M. J. Wright, S. D. Gensemer, J. Vala, R. Kosloff, and P. L. Gould, *Phys. Rev. Lett.* **95**, 063001 (2005).
- [17] T. Brixner and G. Gerber, *ChemPhysChem* **4**, 418 (2003).
- [18] H. Rabitz, R. de Vivie-Riedle, M. Motzkus, and K. Kompa, *Science* **288**, 824 (2000).
- [19] W. Salzmann, U. Poschinger, R. Wester, M. Weidemüller, A. Merli, S. M. Weber, F. Sauer, M. Plewicky, F. Weise, A. Mirabal Esparza, L. Woeste, and A. Lindinger, *Phys. Rev. A* **73**, 023414 (2006).
- [20] B. L. Brown, A. J. Dicks, and I. A. Walmsley, e-print physics/0509109.
- [21] T. Udem, J. Reichert, R. Holzwarth, and T. W. Hänsch, *Phys. Rev. Lett.* **82**, 3568 (1999).
- [22] A. Marian, M. C. Stowe, J. R. Lawall, D. Felinto, and J. Ye, *Science* **306**, 2063 (2004).
- [23] J. Weiner, V. S. Bagnato, S. Zilio, and P. S. Julienne, *Rev. Mod. Phys.* **71**, 1 (1998).
- [24] F. Masnou-Seeuws and P. Pillet, *Adv. At., Mol., Opt. Phys.* **47**, 53 (2001).
- [25] M. Machholm, A. Giusti-Suzor, and F. H. Mies, *Phys. Rev. A* **50**, 5025 (1994).
- [26] A. Vardi, D. Abrashkevich, E. Frishman, and M. Shapiro, *J. Chem. Phys.* **107**, 6166 (1997).
- [27] C. P. Koch, E. Luc-Koenig, and F. Masnou-Seeuws, *Phys. Rev. A* **73**, 033408 (2006).
- [28] H. Wang, P. L. Gould, and W. C. Stwalley, *J. Chem. Phys.* **106**, 7899 (1997).
- [29] C. Amiot, O. Dulieu, and J. Vergès, *Phys. Rev. Lett.* **83**, 2316 (1999).
- [30] V. Kokouline, O. Dulieu, R. Kosloff, and F. Masnou-Seeuws, *J. Chem. Phys.* **110**, 9865 (1999).
- [31] O. Dulieu and F. Masnou-Seeuws, *J. Opt. Soc. Am. B* **20**, 1083 (2003).
- [32] M. Aymar and O. Dulieu (unpublished).
- [33] M. Aymar and O. Dulieu, *J. Chem. Phys.* **122**, 204302 (2005).
- [34] A. Marte, T. Volz, J. Schuster, S. Dürr, G. Rempe, E. G. M. van Kempen, and B. J. Verhaar, *Phys. Rev. Lett.* **89**, 283202 (2002).
- [35] R. F. Gutterres, C. Amiot, A. Fioretti, C. Gabbanini, M. Mazzoni, and O. Dulieu, *Phys. Rev. A* **66**, 024502 (2002).
- [36] K. Willner, O. Dulieu, and F. Masnou-Seeuws, *J. Chem. Phys.* **120**, 548 (2004).
- [37] J. Cao, C. J. Bardeen, and K. R. Wilson, *Phys. Rev. Lett.* **80**, 1406 (2000).
- [38] V. Kokouline, O. Dulieu, and F. Masnou-Seeuws, *Phys. Rev. A* **62**, 022504 (2000).
- [39] V. Kokouline, O. Dulieu, R. Kosloff, and F. Masnou-Seeuws, *Phys. Rev. A* **62**, 032716 (2000).
- [40] N. Spiess, Ph.D. thesis, Universität Kaiserslautern, 1989.
- [41] C. M. Dion, C. Drag, O. Dulieu, B. Laburthe Tolra, F. Masnou-Seeuws, and P. Pillet, *Phys. Rev. Lett.* **86**, 2253 (2001).
- [42] M. R. Manaa, A. J. Ross, F. Martin, P. Crozet, A. M. Lyyra, L. Li, C. Amiot, and T. Bergeman, *J. Chem. Phys.* **117**, 11208 (2002).
- [43] T. Bergeman, C. E. Fellows, R. F. Gutterres, and C. Amiot, *Phys. Rev. A* **67**, 050501(R) (2003).
- [44] C. Gabbanini, A. Fioretti, A. Lucchesini, S. Gozzini, and M. Mazzoni, *Phys. Rev. Lett.* **84**, 2814 (2000).
- [45] J. Ye (private communication).
- [46] C. P. Koch, F. Masnou-Seeuws, and R. Kosloff, *Phys. Rev. Lett.* **94**, 193001 (2005).
- [47] C. P. Koch, J. P. Palao, R. Kosloff, and F. Masnou-Seeuws, *Phys. Rev. A* **70**, 013402 (2004).